

# In situ pH within particle beds of bioactive glasses

Di Zhang, Mikko Hupa, Leena Hupa\*

*Process Chemistry Centre, Åbo Akademi University, Piispankatu 8, FI-20500 Turku, Finland*

Received 16 January 2008; received in revised form 10 April 2008; accepted 16 April 2008

Available online 28 April 2008

## Abstract

The in vitro behavior of three bioactive glasses with seven particle size distributions was studied by measuring the in situ pH inside the particle beds for 48 h in simulated body fluid (SBF). After immersion, the surface of the particles was characterized with a field emission scanning electron microscope equipped with an energy-dispersive X-ray analyzer. In addition, the results were compared with the reactions of the same glasses formed as plates. A similar trend in pH as a function of immersion time was observed for all systems. However, the pH inside the particle beds was markedly higher than that in the bulk SBF of the plates. The pH decreased as power functions with increasing particle size, i.e. with decreasing surface area. The in vitro reactivity expressed as layer formation strongly depended on the particle size and glass composition. The average thickness of the total reaction layer decreased with the increase in sample surface area. Well-developed silica and calcium phosphate layers typically observed on glass plates could be detected only on some particles freely exposed to the solution. No distinct reaction layers were observed on the finest particles, possibly because the layers spread out on the large surface area. Differences in the properties of the bulk SBF and the solution inside the particle bed were negligible for particles larger than 800  $\mu\text{m}$ . The results enhance our understanding of the in vitro reactions of bioactive glasses in various product forms and sizes.

© 2008 Acta Materialia Inc. Published by Elsevier Ltd. All rights reserved.

**Keywords:** Bioactive glass; Particle size; In vitro test; In situ pH; Reaction layers

## 1. Introduction

Bioactive glasses, developed by Hench represent a group of glasses that can bond to bone by formation of an apatite layer. The formation of the bone-like layer occurs not only in the body, but also in vitro. On immersion of a bioactive glass in an aqueous solution, three general processes occur: leaching, dissolution and precipitation [1]. Fast leaching results in an increase in the pH of the surrounding solution. The pH change has been shown to vary depending on, for example, the glass composition, surface area to volume ratio and sample dosage and agitation rate of the system [2–7]. By studying the pH changes in the solution, a fast and simple determination of the in vitro behavior of the glass can be obtained. After partial leaching and dissolution, silica- and calcium

phosphate-rich layers start to form on the glass surfaces. The ability of glass to form a calcium phosphate layer in vitro is often taken as a measure of its bioactivity in vivo. Banchet et al. [8,9] verified the in vitro formation of silica-rich and calcium phosphate layers on particles of powdered bioactive glasses (<40  $\mu\text{m}$ ) by elemental analysis at the submicrometer scale by scanning transmission spectroscopy associated with energy-dispersive X-ray spectroscopy. Karlsson et al. [10] reported that the solubility of hydroxyapatite depended on temperature, the concentrations of calcium and phosphate and pH. According to them, the silica gel was not stable when the pH increased to above 9.5. However, the stability of the calcium phosphate precipitation increased with pH [10]. According to Lu and Leng, the nucleation rate of calcium phosphate precipitation in simulated body fluid (SBF) was significantly affected by the pH value, resulting in a different crystallized structure of the precipitate [11]. A high pH environment was favorable for hydroxyapatite nucleation,

\* Corresponding author. Tel.: +358 2 215 4563; fax +358 2 215 4962.  
E-mail address: [leena.hupa@abo.fi](mailto:leena.hupa@abo.fi) (L. Hupa).

and the hydroxyapatite nucleation rate approached that of octacalcium phosphate at pH 10 [11].

Many *in vitro* studies of bioactive glasses are carried out with monolithic samples, i.e. disks and plates [4,12–14]. However, various clinical applications also call for other shapes and sizes of bioactive glass products. Glass particulates greater than 100  $\mu\text{m}$  in diameter, which can be used to fill in bone defects, have been investigated by Greenspan et al. and Peltola et al. [16,17]. Bioactive glasses with a porous structure have been studied by Ylänen et al. [18]. In addition, studies on bioactive glass powders with an average particle size significantly smaller than 100  $\mu\text{m}$  have been carried out [19,20]. Fine powders of bioactive glasses have been used as a coating material on high-strength metal implants [21,22]. Fine powders of bioactive glasses in dental paste material have been found to show antibacterial properties for the prevention of infections [23,24]. The antibacterial properties of the powdered bioactive glasses on a wide selection of bacterial species were reported in our previous work [25,26].

The present work discusses the *in vitro* behavior of various particle size fractions of three bioactive glasses. The goal is to establish the influence of particle size on the *in vitro* properties of glasses in SBF. The results are relevant in understanding the influence of particle size on *in vitro* and *in vivo* reactions of bioactive glasses.

## 2. Materials and methods

Two well-known bioactive glasses, 45S5 and S53P4, both used in clinical applications, and one experimental bioactive glass, 23-04, were used in this study (Table 1). Glass 23-04 has been discussed in our previous reports [14,15]. The glasses were made from mixtures of analytical grade  $\text{Na}_2\text{CO}_3$ ,  $\text{K}_2\text{CO}_3$ ,  $\text{MgO}$ ,  $\text{CaCO}_3$ ,  $\text{H}_3\text{BO}_3$ ,  $\text{CaHPO}_4 \cdot 2\text{H}_2\text{O}$  and commercial grade Belgian quartz sand. Batches were melted in a Pt crucible at 1360  $^\circ\text{C}$  for 3 h. After casting and annealing, the glasses were crushed and remelted in order to improve homogeneity. Glass plates with dimensions of  $2.00 \times 1.50 \times 0.15$  cm were cut from the blocks by a low speed diamond saw. The glass blocks were crushed and sieved to give the following size fractions: <45, 45–90, 90–250, 250–315, 315–500, 500–800 and 800–1000  $\mu\text{m}$ . SBF was prepared according to the protocol of Kokubo et al. [27]. The pH of the solution was adjusted to around 7.3 at 37  $^\circ\text{C}$ .

A Teflon container with a cylindrical bottom cavity was used as the container for the *in situ* pH measurements (Fig. 1). A microelectrode (Orion 9863BN) was inserted inside

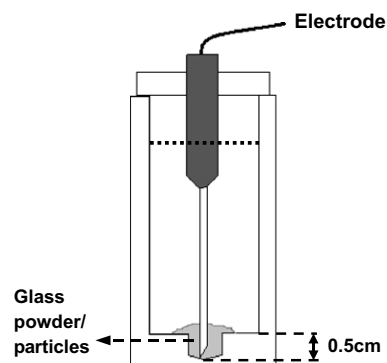


Fig. 1. Experimental scheme showing the *in situ* measurement for glass particles.

the cavity. The total tip length of the electrode was 137 mm and the needle length was 40 mm. The diameters of the upper part and the needle tip were 7.6 and 1.7 mm, respectively. About 1.5 g of glass particles was put into the cavity so that the detecting area of the electrode was totally covered. Then 15 ml SBF was carefully poured into the container to give an approximate sample concentration of 100  $\text{mg ml}^{-1}$ . The pH in the powder bed was measured *in situ* at 37  $^\circ\text{C}$  for 48 h. The pH in the SBF after removing the particles was also measured at 48 h.

The plate samples were placed in a polystyrene container. About 17 ml of SBF was added to the container to give a ratio of surface area of particles to volume of SBF (SA/V) of  $0.4 \text{ cm}^{-1}$ , corresponding to an average concentration of 100  $\text{mg ml}^{-1}$ . The plates were immersed for 4, 8, 24 and 72 h at 37  $^\circ\text{C}$ . The pH in the bulk solutions was measured at 37  $^\circ\text{C}$  with a normal glass electrode after removing the glass plates.

After immersion the samples were washed with ultrapure water and ethanol. The concentration of phosphorus ions in SBF after removing the particles was measured with an inductively coupled plasma-optical emission spectrometer (ICP-OES; Optima 5300 DV, Perkin Elmer) for glasses S53P4 and 23-04 at 2, 4, 27 and 48 h for the finest fraction. Particle samples at 48 h and plate samples at 72 h were analyzed by a field emission scanning electron microscope (LEO 1530) equipped with an energy-dispersive X-ray analyzer (EDXA; ThermoNoram). After embedding in resin, the samples were cut from the middle and the cross-sectional surfaces of the samples were observed.

## 3. Results

The pH of the SBF inside the particle beds and in the bulk solutions after immersing the plates are shown in Fig. 2. The maximum standard deviation of the pH measured was 0.1 pH unit. For both particles and plates, the pH values were highest for glass 45S5 and lowest for 23-04. The pH of the immersion solutions of the plates increased with time, but to a lower degree than for the particle systems. The pH inside the particle beds increased with

Table 1  
Codes and chemical composition (wt.%) of the experimental glasses

Glass	$\text{Na}_2\text{O}$	$\text{K}_2\text{O}$	$\text{MgO}$	$\text{CaO}$	$\text{B}_2\text{O}_3$	$\text{P}_2\text{O}_5$	$\text{SiO}_2$
45S5	24.5	0	0	24.5	0	6	45
S53P4	23	0	0	20	0	4	53
23-04	5	11.25	4.5	20	2	1	56.25

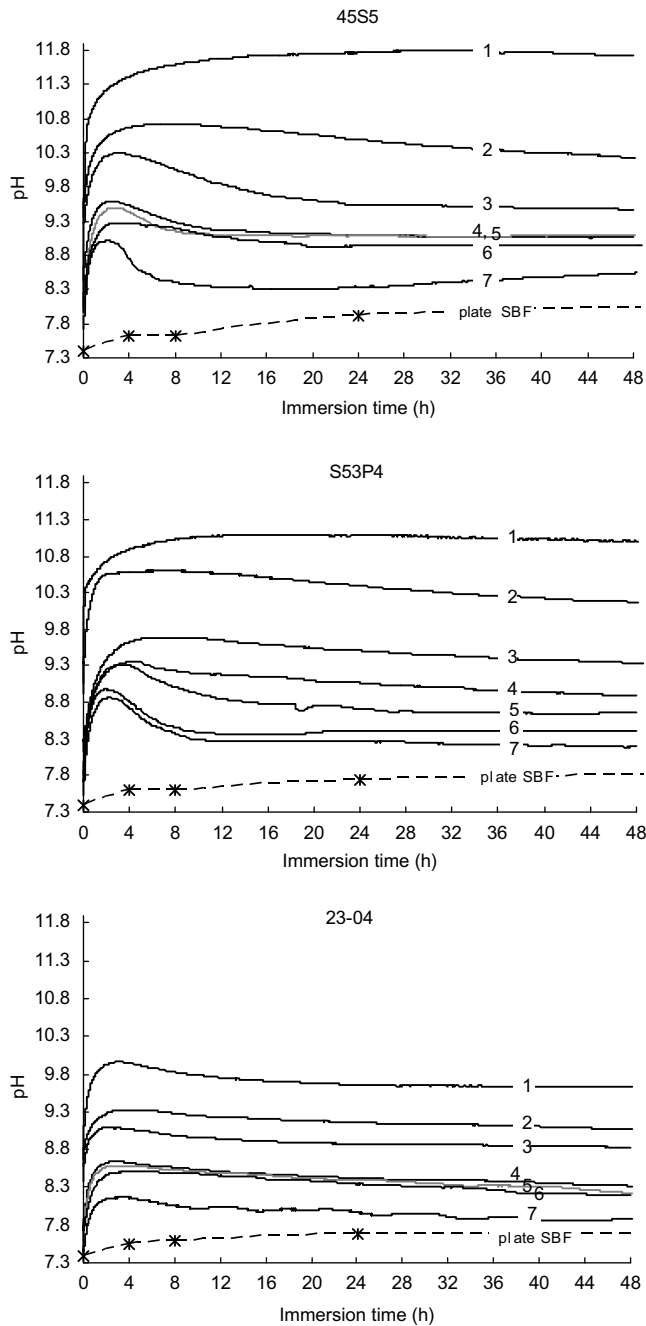


Fig. 2. In situ pH in the SBF inside particle beds during immersion for glasses 45S5, S53P4 and 23-04. The numbers 1–7 present the curves for the average particle sizes: <45, 45–90, 90–250, 250–315, 315–500, 500–800 and 800–1000  $\mu\text{m}$ , respectively. The pH in the mixed immersion solution of glass plates ( $2.00 \times 1.50 \times 0.15 \text{ cm}$ ) is shown by the dashed line as a function of the time points indicated.

immersion time and particle size range, and showed a similar trend for all samples during the in situ measurements. The pH in the samples with the finest particle size (<45  $\mu\text{m}$ ) was much higher than the values for the coarser particle fractions. For all glasses, the largest size fraction (800–1000  $\mu\text{m}$ ) showed a much lower pH value than the other fractions.

The rate of pH increase inside the particle beds depended on particle size and progression of the immer-

sion. The greatest increase in pH was observed during the first 2 h of immersion, and maximum values were seen within 1–4 h. In the bulk immersion solution of the plates, the greatest rate of pH increase was also seen within the first 4 h. With prolonged immersion, the pH inside the particle beds decreased slightly, except for the <45  $\mu\text{m}$  fractions of glasses 45S5 and S53P4. The smaller the particle size, the greater the rate of pH increase during the first 2 h of immersion. In order to estimate the influence of the surface area of the samples on the pH changes, the total surface area of the different particle size fractions was calculated by assuming spherical (or cubic) particles and an average density of  $2.4 \text{ g cm}^{-3}$  for the bioactive glasses. The calculated surface area of the 1.5 g samples as a function of the average particle size is given in Fig. 3. The figure shows that, for the given mass of the sample, the total surface area increases as a power function with decreasing particle size. The average particle size of each fraction was used to estimate the maximum and final values of the bed pH as a function of the calculated surface area (Fig. 4). The figure also shows the final pH in the bulk solutions for glasses 45S5 and S53P4 after removing the particles. The final pH in the bulk solution and inside the particle beds was of the same level only for the lowest surface area, i.e. the largest particle size fraction, while for the fine powders large differences were recorded.

Three reaction layers were seen in the SEM images of the cross-sections of the samples. EDXA indicated that the layers were a silica-rich (Si) layer, a calcium phosphate-rich (CaP) layer and/or a mixed layer (Si + CaP) containing both silica and calcium phosphate. Fig. 5 shows the reaction layers formed on glasses 45S5 and S53P4 after 48 h in SBF. The chemical compositions of the layers are given by the EDXA spectra in Fig. 6. The SEM images on both the top and the cross-sectional surfaces showed that the formation of the reaction layers varied on individual particles. The maximum standard deviation of the thickness of the Si-rich, CaP-rich and mixed layers mea-

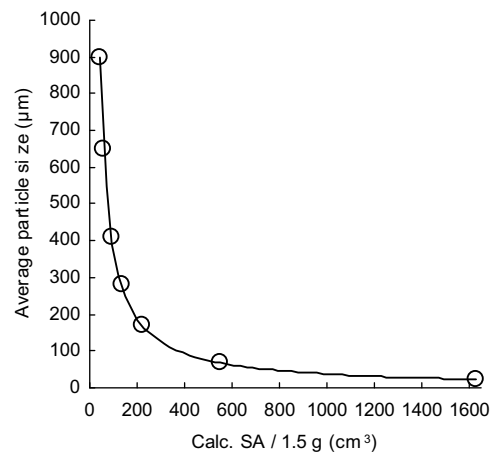


Fig. 3. Average particle size ( $\mu\text{m}$ ) as a function of calculated total surface area ( $\text{cm}^3$ ) of the 1.5 g glass samples by assuming spherical (or cubic) particles and an average density of  $2.4 \text{ g cm}^{-3}$ .

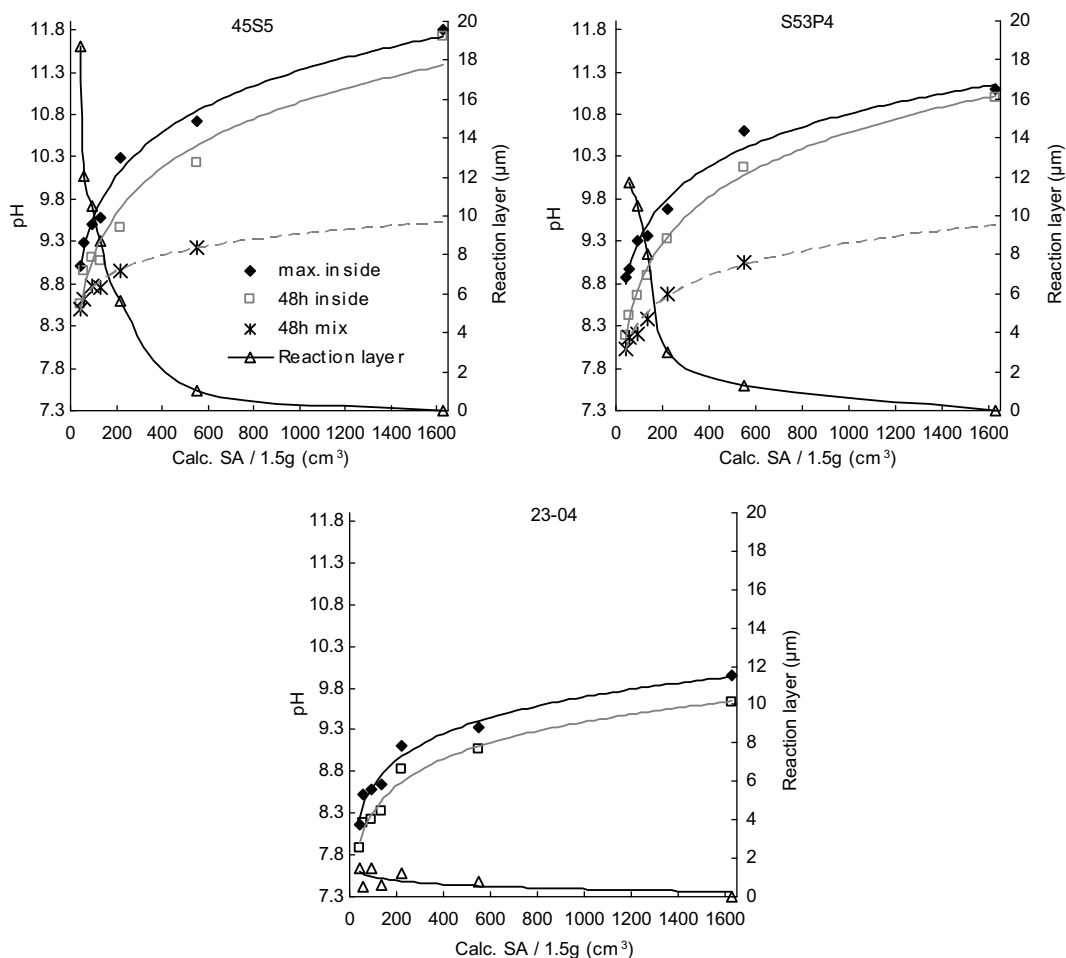


Fig. 4. Maximum (max inside) and final (48 h inside) in situ pH in SBF inside particle beds as a function of calculated surface area (Calc. SA) of a 1.5 g glass sample, and the pH in the final mixed SBF after removing the particles (48 h mix). The average thickness ( $\mu\text{m}$ ) of the reaction layer on the glass surface at 48 h as a function of the Calc. SA is also shown by the secondary y-axis.

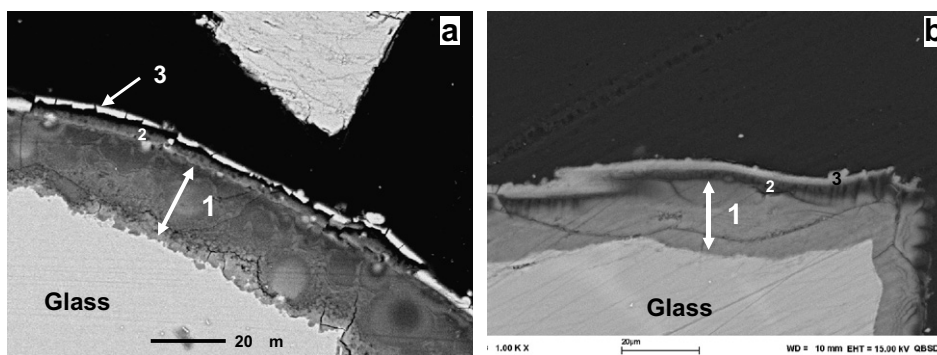


Fig. 5. SEM images of cross-sectional surfaces of glass particles after 48 h in SBF: (a) 45S5, 800–1000  $\mu\text{m}$  and (b) S53P4, 500–800  $\mu\text{m}$ . The numbers indicate the layers as follows – 1: Si-rich layer (Si); 2: mixed layer containing both Si and calcium phosphate (Si + CaP) and 3: calcium phosphate-rich layer (CaP).

sured on the cross-sections of the glasses was  $\pm 1.6$ ,  $\pm 0.7$  and  $\pm 0.2$   $\mu\text{m}$ , respectively. Fig. 7 shows the uneven layer formation on the 250–350  $\mu\text{m}$  particles of glass 45S5. Differences in layer formation were found both between glass compositions and between particle fractions of the same

glass. The thickness ranges of the reaction layers on the different size particles fractions are given in Table 2. On plates, the layers were relatively even and thickness depended on the glass composition. On the smallest particles only thin and sporadic layers or no layers at all could

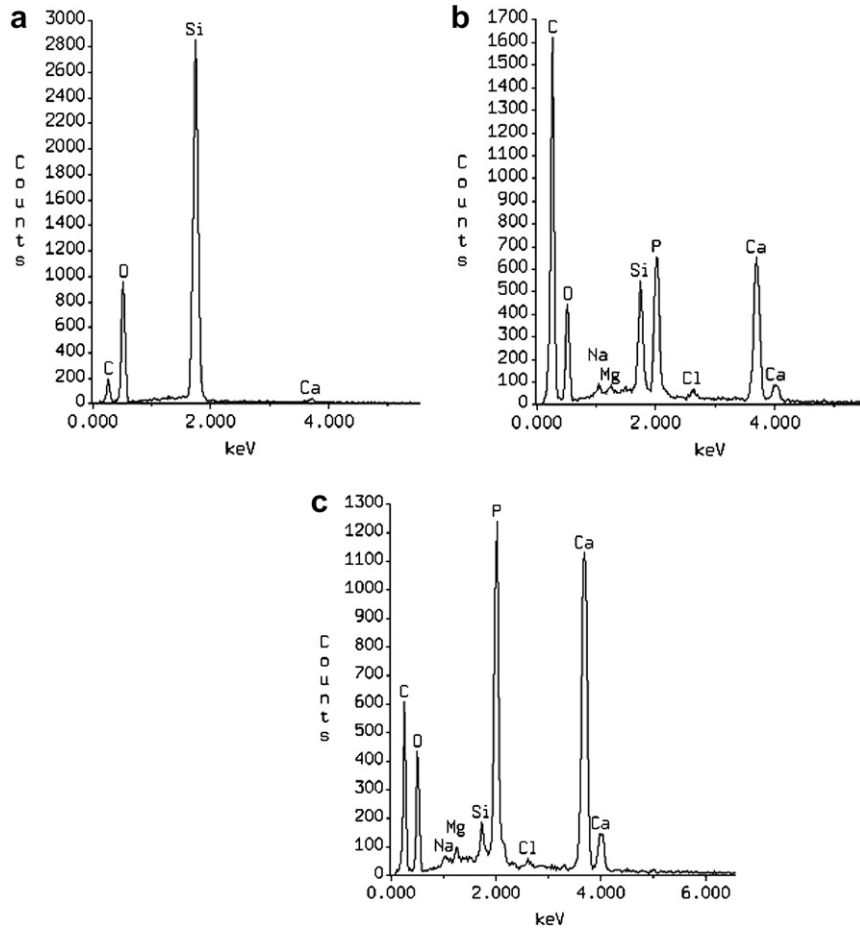


Fig. 6. EDXA spectra showing the compositions of the three layers indicated in Fig. 5b for S53P4 (500–800  $\mu\text{m}$ ): (a) Si-rich layer (Si); (b) mixed layer containing both Si and calcium phosphate (Si + CaP) and (c) calcium phosphate-rich layer (CaP).

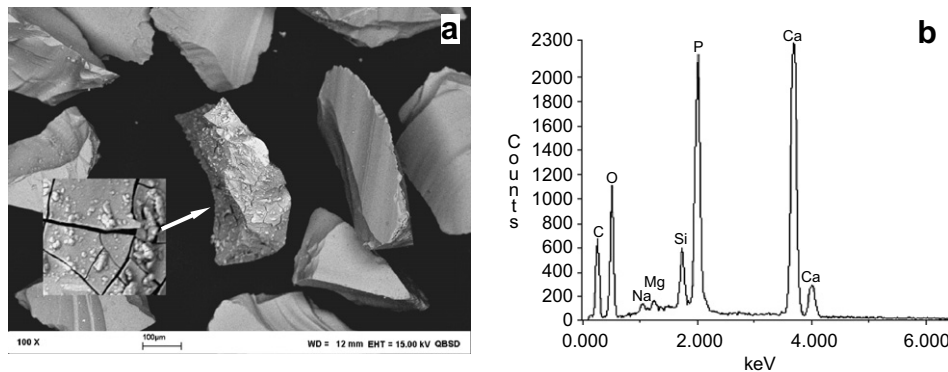


Fig. 7. (a) SEM image of the top surface of glass 45S5, 250–315  $\mu\text{m}$  particles and (b) EDXA spectra of the middle particle in image (a).

be observed. However, the ICP-OES analysis of the immersion solutions of the finest fractions of glasses S53P4 and 23-04 indicated that the phosphorus ion concentration had decreased to one-third of the initial value at 2 h and was very low after 48 h (Fig. 8). The maximum standard deviation of the measured concentration of the phosphorous ion in SBF was  $2.7 \text{ mg l}^{-1}$ . For the samples with an average diameter larger than 250  $\mu\text{m}$ , the surface morphol-

ogy on the tops of the particles showed the clear formation of reaction layers on some of the particles. Generally, the thickness of the reaction layers increased with increasing particle size. Clearly thicker layers were found on particles of glasses 45S5 and S53P4 than on 23-04. These results were in accordance with our previous results, i.e. glasses 45S5 and S53P4 showed a high in vitro bioactivity while glass 23-04 had a clearly lower bioactivity [14].

Table 2  
Reaction layer thicknesses ( $\mu\text{m}$ ) measured on cross-sectional surface of the particles (48 h in SBF) and on plates (72 h in SBF)

Glass	Layers ( $\mu\text{m}$ )	Particle size ( $\mu\text{m}$ ) (48 h)							Plate (72 h)
		<45	45–90	90–250	250–315	315–500	500–800	800–1000	
45S5	Si	0	0–2.1	0–10.0	0–14.0	0–20.0	0–20.0	0–30.0	9.6–12.8
	Si + CaP	0	0	0–1.3	0	0	0–1.1	0–4.0	0.2–0.6
	CaP	0	0	0	0–3.4	0–1.0	0–3	0–3.5	2.1–3.5
S53P4	Si	0	0–2.5	0–5.0	0–15.0	0–20.0	0–19.0	0–7.0	3.0–8.7
	Si + CaP	0	0	0–1.0	0	0–1.0	0–1.0	0–1.0	0–2.5
	CaP	0	0	0	0–1.1	0	0–3.5	0	1.6–2.9
23-04	Si	0	0–1.5	0–2.5	0–1.0	0–2.5	0–1.0	0–1.5	1.1–1.4
	Si + CaP	0	0	0	0–0.3	0	0	0–1.5	
	CaP	0	0	0	0	0–0.5	0	0	0

Si: Si-rich layer; Si + CaP: mixed layer containing both Si and calcium phosphate and CaP: calcium phosphate-rich layer.

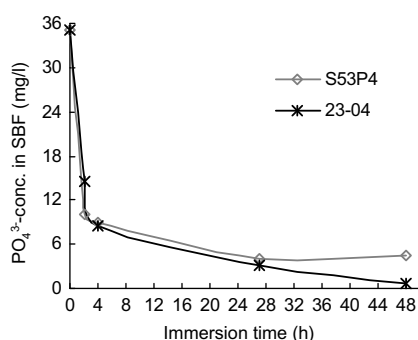


Fig. 8. Concentration of phosphorous ions as a function of immersion time after removing the particles (<45  $\mu\text{m}$ ) from SBF for glasses S53P4 and 23-04.

#### 4. Discussion

In general, the reactions of the glass particles followed the steps proposed by Hench et al. [1]. The particles started to leach and dissolve immediately when in contact with SBF. The rapid release of alkali ions was assumed to cause the similarly rapid increase in pH inside the powder beds and in the bulk solution. For all three compositions, the fastest pH increase was observed within the first 4 h of immersion, after which the pH at the glass–solution interface was almost constant or decreased slightly, depending on the glass composition and particle size. With prolonged immersion, the rapid increase in the interfacial pH was slowed down by the reaction layers that developed on the glass surfaces, as suggested by the SEM observations. The pH changes measured in this study were in good agreement with observations of immersion of glass 45S5 particles in Tris-buffered solutions by Cerruti et al. and Greenspan et al. [2,3], in which a rapid increase in pH took place in the solution during the first 2–6 h, after which the pH either gradually increased or slightly decreased.

As shown in Fig. 4, the pH values increased with the total surface area as a power function, i.e. with decreasing average particle size. Poor diffusion in the static experimental conditions was assumed to give a supersaturated solu-

tion inside the particle beds within the first few hours of immersion. For the systems with fine powder (<45  $\mu\text{m}$ ), the diffusion between the solution inside the particle beds and the bulk solutions was poorest, as indicated by the large differences in the final pH values of the bulk and interfacial solutions (Fig. 4). In contrast, the largest particles did not markedly prevent diffusion between the ions inside the particle bed and bulk SBF. The higher pH values obtained with the smaller particles depended on their large surface area. The bigger the particles, the smaller the differences between the pH values.

The formation of the layers on the particles strongly depended on the particle size, glass composition and local environment around the particles. As given in Fig. 7, after 48 h in SBF a calcium phosphate layer formed on some particles only. The difference in the layer formation was assumed to depend on the ion concentration of the SBF to which the particles had been exposed, i.e. either a supersaturated solution inside the bed or the bulk solution at the bed interface. The particles at the bed interface were assumed to show distinct reaction layers, while inside the bed layers could not be verified. Similar results based on Fourier transform infrared spectra of the reaction layers on bioactive glass particles have been reported by Hench et al. [28]. Differences in reaction layers were assumed to depend on uneven exposure of the particles to the solution in the container. In our previous study, the reaction layers formed in SBF on a bundle of bioactive glass fibers were found to vary with the location of the individual fibers in the bundle [29]. The outer fibers had clear and uniform layers, while the surfaces inside the bundles showed no or uneven reaction layers. Thus, poor diffusion was assumed to give a high local pH inside the particle bed. At this condition, the silica gel was unstable [10]. The high pH should increase the stability of the calcium phosphate precipitation [10]. However, due to the high SA/V ratio inside the bed, a distinct calcium phosphate layer could not be detected on individual particles by SEM.

The particle size had a strong impact on the in vitro behavior of the glasses. Bigger particles showed a smaller increase in pH but more clear reaction layers than particles

smaller than 250  $\mu\text{m}$ . The smaller the size fraction, the higher the SA/V ratio. Generally, the average thickness of the total reaction layer, given as the sum of the average thickness of the three layers, decreased with the total surface area of the sample, i.e. with decreasing particle size (Fig. 4). Similar phenomena have been observed by other researchers. According to Greenspan et al. [2], higher SA/V ratios gave faster and larger increases in pH and rapid initial layer formation, but less-developed calcium phosphate layers than lower SA/V ratios. Cerruti et al. [3] also observed that smaller particles gave a faster cation release, a higher solution pH and a thinner calcium phosphate layer. Greenspan et al. [2] assumed that the poor layer formation on the smaller particles was due to the rapid increase in pH, which altered the solubilization and subsequent repolymerization of the Si-rich layer, which is necessary to form the calcium phosphate layer. The high surface area itself could also be an important reason for the less-developed reaction layers. Clear calcium phosphate layers could not be seen by SEM/EDXA for the fraction smaller than 45  $\mu\text{m}$ , although phosphorous ions in the SBF were clearly consumed during immersion. This suggested that precipitation of calcium phosphate also took place in the sample with the finest powder. The calcium phosphate was assumed to precipitate and spread out on the large surface area in a layer that was too thin to be verified by SEM. However, the formation of silica-rich and calcium phosphate layers on fine particles of bioactive glasses (<40  $\mu\text{m}$ ) was observed when using a much lower sample concentration (2 mg ml<sup>-1</sup>), i.e. a lower SA/V ratio [8,9]. As no essential differences between the layers on individual particles were reported, the low sample concentration was likely to provide unhindered diffusion between the particle interfaces and the solution. In this work, it was found that the finer the fraction, the poorer the diffusion between the solution inside the particle bed and the bulk solution, thus giving less-developed reaction layers on the particles inside the bed.

## 5. Conclusions

In vitro reactions of bioactive glasses in different product forms, ranging from fine powder to different particle size fractions within 45–1000  $\mu\text{m}$ , were compared with reaction layers observed on plates of the same glasses. The in vitro behavior of glass particles strongly depended on the particle size, glass composition and local environment around the separate particles. For the same concentration a finer fraction gives a higher pH value than a coarser fraction. The pH in the solution inside the particle bed was much higher than that in the bulk solution. The difference in surface area was assumed to explain the trend of pH change as a function of particle size. With the largest size fraction, no differences in the final pH between the bulk and interior solutions could be observed. Distinct reaction layers typical for glass plates were observed only on some particles, which were assumed to be exposed to

bulk SBF. With increasing particle size, the change in solution pH was less, while more distinct layers on particle surfaces were seen. The largest size fractions gave results similar to those obtained with plates of bioactive glasses. For the finest fraction, <45  $\mu\text{m}$ , no layers could be observed due to the large surface area. Thus, in vitro layer formation on particles of bioactive glasses is likely to give similar results with monoliths only when using large size fractions.

## Acknowledgements

This work is part of the activities of the Åbo Akademi Process Chemistry Centre, the National Centre of Excellence Programme of the Academy of Finland. The Finnish Funding Agency for Technology and Innovation (Tekes) and the Graduate School of Materials Research (GSMR) are acknowledged for financial support.

## References

- [1] Hench LL, Andersson Ö. Chapter 3: bioactive glasses. In: Hench LL, June Wilson, editors. An introduction to bioceramics. Bioactive glasses. Singapore: Springer; 1993. p. 41–62.
- [2] Greenspan DC, Zhong IP, La Torre GP. Effect of surface area to volume ratio on in vitro surface reactions of bioactive glass particulates. *Bioceramics* 1994;7:55–60.
- [3] Cerruti MG, Greenspan D, Powers K. An analytical model for the dissolution of different particle size samples of bioglass® in TRIS-buffered solution. *Biomaterials* 2005;26:4903–11.
- [4] Peitl O, Zanolto ED, Hench LL. Highly bioactive P<sub>2</sub>O<sub>5</sub>-Na<sub>2</sub>O-CaO-SiO<sub>2</sub> glass-ceramics. *J Non-Cryst Solids* 2001;292:115–26.
- [5] Jones JR, Sepulveda P, Hench LL. Dose-dependent behavior of bioactive glass dissolution. *J. Biomed Mater Res: Appl Biomater* 2001;58:720–6.
- [6] Rámila A, Vallet-Regí M. Static and dynamic in vitro study of a sol-gel glass bioactivity. *Biomaterials* 2001;22:2301–6.
- [7] Cerruti M, Greenspan D, Powers K. Effect of pH and ionic strength on the reactivity of Bioglass® 45S5. *Biomaterials* 2005;26:1665–74.
- [8] Banchet V, Jallot E, Michel J, Wortham L, Laurent-Maquin D, Balossier G. X-ray microanalysis in STEM of short-term physicochemical reactions of bioactive glass particle/biological fluid interface. Determination of O/Si atomic ratios. *Surf Interf Anal* 2004;36:658–65.
- [9] Banchet V, Michel J, Jallot E, Wortham L, Bouthors S, Laurent-Maquin D, et al. Interfacial reactions of glasses for biomedical application by scanning transmission electron microscopy and microanalysis. *Acta Biomater* 2006;2:349–59.
- [10] Karlsson KH, Backman R, Hupa M. An equilibrium study of phosphate precipitation in bioactive glass. *Key Eng Mater* 2002;218–220:103–7.
- [11] Lu X, Leng Y. Theoretical analysis of calcium phosphate precipitation in simulated body fluid. *Biomaterials* 2005;26:1097–108.
- [12] Andersson Ö, Vähätalo K, Yli-Urpo A, Happonen R-P, Karlsson KH. Short-term reaction kinetics of bioactive glass in simulated body fluid and in subcutaneous tissue. *Bioceramics* 1994;7:67–72.
- [13] Rehman I, Knowles JC, Bonfield W. Analysis of in vitro reaction layers formed on Bioglass® using thin-film X-ray diffraction and ATR-FTIR microspectroscopy. *J Biomed Mater Res: Appl Biomater* 1998;41:162–6.
- [14] Zhang D, Vedel E, Hupa L, Aro HT, Hupa M. Predicting physical and chemical properties of bioactive glasses from chemical composition. Part III. In vitro reactivity. *Glass Technol – Part A* [in press].

- [15] Vedel E, Zhang D, Arstila H, Hupa L, Hupa M. Predicting physical and chemical properties of bioactive glasses from chemical composition. Part IV. Tailoring compositions with desired properties. *Glass Technol – Part A* [in press].
- [16] Greenspan DC, Zhong JP, La Torre GP. The evaluation of surface structure of bioactive glasses in vitro. *Bioceramics* 1995;8:477–88.
- [17] Peltola M, Suonpää J, Aitasalo K, Andersson Ö, Määttä H, Yli-Urpo A. Long-term reactions in vitro with bioactive glass S53P4. *Bioceramics* 1998;11:477–88.
- [18] Ylänen H, Karlsson K, Itälä KH, Aro HT. Effect of immersion in SBF on porous bioactive bodies made by sintering bioactive glass microspheres. *J Non-Cryst Solids* 2000;275:107–15.
- [19] Rizkalla AS, Jones DW, Routledge T, Hall GC, Langman M. Chemical reactivity of experimental bioactive glasses. *Bioceramics* 1998;11:133–6.
- [20] Salinas AJ, Román J, Vallet-Regi M, Oliveira JM, Correia RN, Fernandes MH. In vitro bioactivity of glass and glass-ceramics of the  $3\text{CaO} \cdot \text{P}_2\text{O}_5\text{-CaO} \cdot \text{SiO}_2\text{-CaO} \cdot \text{MgO} \cdot 2\text{SiO}_2$  system. *Biomaterials* 2000;21:251–7.
- [21] Ferraris M, Verné E, Appendino P, Moisescu C, Krajewski A, Ravaglioli A, et al. Coatings on zirconia for medical applications. *Biomaterials* 2000;21:765–73.
- [22] Vedel E, Moritz N, Ylänen H, Jokinen M, Hupa M, Yli-Urpo A. Creation of bioactive glass coating on titanium by local laser irradiation. Part II. Effect of the irradiation on the bioactivity of the glass. *Key Eng Mater* 2003;240–242:225–8.
- [23] Zehnder M, Waltimo T, Sener B, Söderling E. Dentin enhances the effectiveness of bioactive glass S53P4 against a strain of *Enterococcus faecalis*. *Oral Surg Oral Med Pathol Oral Radiol Endod* 2006;101:530–5.
- [24] Stoor P, Söderling E, Salonen JI. Antibacterial effects of a bioactive glass paste on oral microorganisms. *Acta Odontol Scand* 1998;56:161–5.
- [25] Munukka E, Leppäranta O, Vaahtio M, Peltola T, Zhang D, Hupa L, et al. Bactericidal effect of bioactive glasses on clinically important aerobic bacteria in vitro. *J Mater Sci: Mater Med* 2008;19(1):27–32.
- [26] Leppäranta O, Vaahtio M, Peltola T, Zhang D, Hupa L, Hupa M, et al. Antibacterial effect of bioactive glasses on clinically important anaerobic bacteria in vitro. *J Mater Sci: Mater Med* 2008;19(2):547–51.
- [27] Kokubo T, Kushitani H, Sakka S, Kitsugi T, Yamamuro T. Solutions able to reproduce in vivo surface-structure changes in bioactive glass-ceramic A–W. *J Biomed Mater Res* 1990;24:721–34.
- [28] Warren DL, Clark EA, Hench LL. An investigation of bioglass powders: quality assurance test procedure and test criteria. *J. Biomed Mater Res: Appl Biomater* 1989;23:201–9.
- [29] Zhang D, Arstila H, Vedel E, Ylänen H, Hupa L, Hupa M. In vitro behavior of fiber bundles and particles of bioactive glasses. *Key Eng Mat* 2008;361–363:225–58.